# Fabrication of a Multi-Physics Integral Structural Diagnostic System Utilizing Nano-Engineered Materials

Seth S. Kessler[1], Ajay Raghavan[1], Christopher T. Dunn[1],
Sunny S. Wicks[2], Roberto Guzman deVilloria[2] and Brian L. Wardle[2]

[1] *Metis Design Corporation, Cambridge, MA, 02141, USA*
*skessler@metisdesign.com*
*ajay@metisdesign.com*
*cdunn@metisdesign.com*

[2] *Massachusetts Institute of Technology, Cambridge, MA, 02139, USA*
*swicks@mit.edu*
*rguzman@mit.edu*
*wardle@mit.edu*

## ABSTRACT

Composites present additional challenges for inspection due to their heterogeneity and anisotropy, and since damage often occurs beneath their surface. Currently successful laboratory non-destructive methods, such as X-ray and C-scans, are impractical for inspection of large integrated structures. It is clear that new approaches for inspection of composites need to be developed. During the present research, multiple carbon nanotube (CNT) based NDE & SHM techniques were investigated to resolve these issues. Aligned CNTs offer excellent mechanical toughness improvements for traditional composite laminates, and additionally enable multifunctional capabilities through piezoresistive properties and greatly enhanced electrical and thermal conductivity. This paper introduces the fabrication of fuzzy-fiber reinforced plastic (FFRP) composite laminates uses CNTs, and presents results for multiple CNT-enhanced laminates that were electroded using direct-write techniques and subject to impact damage. A resistive-based method was used to create a detailed damage map of the effected zone. Finally, demonstrations are also described for multiple alternative CNT-based NDE approaches that were explored.*



## 1 INTRODUCTION

Advanced composite materials are being adopted increasingly in structural design due to their superior specific stiffness and strength, resistance to fatigue, corrosion and ability to reduce part count. Traditional composites, however, exhibit significantly reduced electrical and thermal conductivity relative to metals, and matrix-rich regions at ply interfaces results in poor interlaminar properties. Additionally, sustained damage in composites is often not visible, complicating assessment of structural integrity. Recent efforts to address damage detection in advanced composites include the incorporation of carbon nanotubes (CNTs).

Several studies have shown that CNTs possess exceptional mechanical stiffness (as high as ~1 TPa) and strength, as well as excellent electrical conductivity (~1000x copper) and piezoresistivity (resistivity change with mechanical strain). Thus, in principle, they could be used not only to reinforce composite structures for improved impact and delamination resistance, but also to enable multifunctional structures with structural health monitoring (SHM) capability. SHM implies a system integrated with a structure to provide continuous remote monitoring for damage.

The present work builds on a hybrid composite architecture—fuzzy-fiber reinforced polymer (FFRP)—that strategically places aligned CNTs throughout the laminate. Here, multifunctional attributes of FFRP are explored to assess the potential of damage detection using enhanced electrical conductivity of the laminate. Damage increases resistance to electrical conduction, and therefore changes in both in-plane and through-thickness resistance can be used to sense damage, yielding a non-destructive 3D tomographic view of the damage state in the material.

## 2 BACKGROUND

In the use of CNTs purely to enhance mechanical properties, technical and manufacturing issues have hindered the development of large-scale CNT-enhanced composite structures. Alignment, dispersion and adhesion of CNTs in polymer matrices are vital for structural composite applications, and numerous studies have reported on the difficulties in dispersing CNTs in polymers. These difficulties are further exacerbated when CNT-enhanced matrices are introduced into typical aligned-fiber advanced composites, where the CNT-containing matrix must effectively impregnate a high volume fraction of advanced fibers. Due to issues such as agglomeration and poor dispersion, only marginal improvements in mechanical properties were observed for both nanocomposites, and hybrid composites (in the latter, advanced reinforcing fibers such as carbon are used, unlike in the former), when CNTs are introduced into the bulk matrix. Somewhat better results were achieved using nanoscale modification of the interface between composite plies, by growing CNTs on the surface of cloth or placing unaligned CNTs at low volume fractions on fibers (including at the ply interface). However, these approaches do not significantly improve electrical conductivity and thus cannot exploit the potential multi-functionality of the embedded CNTs.

Electrically-conductive CNT hybrid composites have been designed by some research groups, but most have significant repeatability problems due to factors such as low volume-fraction and poor dispersion. Thostenson and Chou built CNT-enhanced advanced fiber-reinforced composites with improvements in electrical conductivity and had encouraging results in damage monitoring using passive in-plane electrical resistance measurements. However, their approach to incorporating CNTs in the fiber-reinforced composite results in random CNT morphology, resulting in no significant improvement in mechanical properties such as stiffness and strength. Also, their proposed approach to SHM used only in-plane resistance measurement; while this is feasible for coupon-level testing, their approach would require a dense network of invasive wiring and instrumentation for large-area monitoring. Thus, a novel approach to incorporating CNTs in fiber-reinforced aerospace structural composites for SHM is needed, which can fully exploit all the potential advantages of CNTs for improving mechanical properties as well as enable SHM with a non-invasive electrode network.

To address these requirements, the present investigators have developed advanced multifunctional fiber-reinforced laminates with aligned CNTs grown in-situ using a non-invasive electrode network for SHM. Laminates developed through the Nano-Engineered Composite aerospace Structures (NECST) Consortium have already been demonstrated to have as high as 69% higher interlaminar shear strength and much greater electrical conductivity ($10^8$ x through-thickness & $10^6$ x in-plane) compared to similar laminates without CNTs. The Laminates are a three-part hybrid system, as shown in Figure 1: advanced fibers (diameter of order microns) organized in tows and woven, a thermoset polymer resin, and dense aligned CNTs (with mass fraction between 0.5 and 2.5%) organized within the polymer matrix. As illustrated in Figure 1, CNTs are organized radially around the existing micron-sized fibers to form “fuzzy fibers” (FF), and the polymeric matrix binds all the filaments (advanced fibers and CNTs) together to form a fuzzy fiber reinforced plastic (FFRP). The alignment and dispersion of CNTs within the dense array of woven tows and fibers in the cloth material is achieved by radial in situ growth of CNTs from the surface of the woven fibers. The CNTs reinforce the polymer matrix between the advanced fibers to provide enhanced strength and toughness, as well as an electrically conductive pathway, as illustrated in Figure 1.

Resistive sensing methods—essentially putting a voltage across individual conductive fiber bundles and monitoring the change in resistance—have been investigated by previous researchers. However, these methods have been hindered by several factors, including the fact that conventional carbon fibers have significant conductivity variability, changes have been small, and interconnection issues (*i.e.*, measurements from fibers without a free edge). This paper presents an experimental application of CNTs that eliminates both of these problems with increased, reproducible conductivity properties, and offering electrical break-out connections through 3-D surface leads.

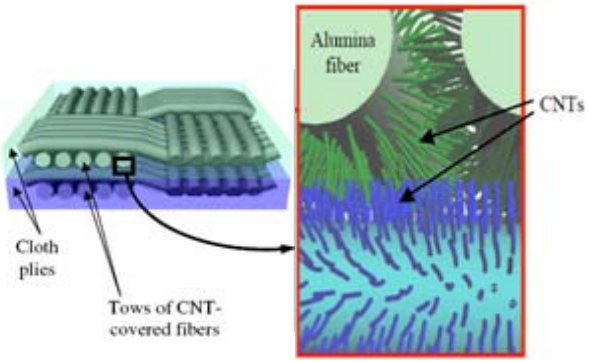


Figure 1: Illustration of FFRP. (Left) Schematic of architecture composed of cloth containing fiber tows covered by CNTs, in matrix. (Right) Closer view of interface cross-section between 2 plies. CNTs grown on surface of each fiber interact with CNTs of nearby fibers achieving inter/intralaminar reinforcement.

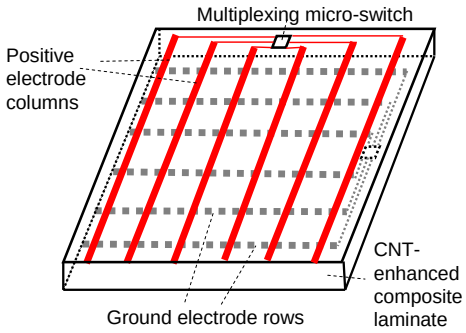


Figure 2: Schematic of non-invasive silver ink electrode and multiplexing switch network for resistance measurements over the FFRP laminate.

## 3 EXPERIMENTAL SETUP

The present investigators leveraged prior experience to instrument FFRP laminates with aligned CNT with a non-invasive silver-ink electrode grid and multiplexing micro-switches connected to compact hardware for resistance measurement. The painted electrode grid, inspired by flat panel liquid crystal display (LCD) technology, use an "active" layer of electrode columns on one surface of the laminate as positive electrode, and on the other surface, another layer of electrode rows will act as "passive" ground (Figure 2). Thus, by selecting a particular row and column, local through-thickness resistance measurements can be obtained for a grid of points over the structure. Furthermore, in-plane surface resistivity changes at a grid point can be obtained by probing resistance between 2 adjacent traces pairs closest to the point on either surface. As one would intuitively expect, damage in the form of delaminations or cracks will affect the CNT link network around the affected zone, and correspondingly the local resistivity. Owing to the presence of the electrode network, by interpolating from the measurements at distinct grid points, high-resolution resistance maps over large structural areas can be obtained, allowing accurate localization of damage.

### 3.1 Proof-of-Concept Demonstration

Manufacturing FFRP laminates involves growing CNTs directly on fibers—in the present case an alumina fiber woven cloth—using a modified thermal chemical vapor deposition (CVD) method developed in previous work. A thick alumina fiber satin-weave cloth is first dipped in a solution of 50mM iron nitrate in isopropanol for 5 minutes and dried in air for at least 8 hours. This catalyst application method allows the catalyst to coat fibers inside the tows of the ply, ultimately distributing CNT growth to all areas of the woven ply. In a CVD furnace, the catalyst is conditioned to form nanoparticles, or seeds, from which CNTs grow radially aligned and perpendicular to the surface of the fibers. They extend into the matrix to provide reinforcement both within each ply (intralaminar) and between plies (interlaminar). The CNTs grown are typically 20 to 50 μm in length, longer than interlaminar spacing (~ 10 μm) and intralaminar spacing (~ 1-5 μm).

FFRP laminates were fabricated using hand layup, the matrix system used was West Systems™ Epoxy, Resin 105 and Hardener 206. In hand layup, a ply is laid down on a sheet of non-porous teflon (GNPT) and epoxy is coated over the surface. The epoxy is wicked into the interior of the woven ply within a few seconds after which another ply is placed on top. In this work, once two plies are stacked, porous Teflon (PT), absorbent bleeder paper, and GNPT are placed over the laminate. A caul plate and vacuum are then used to provide pressure to the assembly to ensure uniform thickness. The sample is then left to cure for 12 hours at room temperature. The resulting specimens have less than 2% void fraction and a fiber volume fraction of ~50%. The resulting composites are trimmed with a diamond-grit wet cutting wheel.

Initially a single FFRP laminate (114 x 25 x 3 mm) was tested to prove the concept. Silver-ink electrodes were painted onto the specimen surfaces using simple tape masks (Figure 3). On the top plate surface, 14 parallel conductors were patterned in the short-dimension. On the opposite surface, 4 parallel conductors were patterned in the long dimension (so that they were perpendicular to the top side conductors through the thickness). These traces were all 1.5 mm wide and spaced 3 mm edge-to-edge. Prior to testing, the electrical resistance was measured using a Fluke 189 model multimeter with resolution 0.01 Ω and accuracy of ±0.05%. Initial data showed significant variability when probing directly on the silver traces. Subsequently, a procedure was developed to bond thick gauge wires to the traces using silver epoxy, resulting in < 1% change (< 0.1 Ω for ~10 Ω trace) across 10 repeat trials. The specimen was centrally impacted with a 13 mm diameter steel ball at using a guided dropped weight to initiate damage. Following impact, post-damage resistance measurements were collected again for each possible combination.

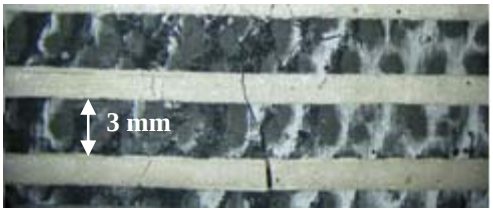


Figure 3: Photograph under microscope of impacted region of FFRP laminate. Painted silver electrodes are 1.5 mm wide and spaced 3 mm edge-to-edge.

### 3.2 Validation Demonstration

Following the proof-of-concept test, 3 further FFRP laminates were then tested to validate the initial results using a refined setup, which improved several elements of the process. First, the silk-screening process was improved to reduce trace resistance & variability, both of which improved measurement accuracy. This was accomplished by selecting a slightly different silver formulation, as well as testing various measurement thicknesses to determine an appropriate value that increases repeatability and was less sensitive to layer tolerances. A chemical etched template was used to apply the proper pattern with better precision. More traces were applied to these specimens increased spacial resolution (32 horizontal and 8 vertical as opposed to 14 x 4) by greater than a factor of 4. All traces were 1.5 mm wide and also spaced by 1.5 mm.

Next, rather than using soldered wires connect to the traces, a single double-sided copper-coated-Kapton w/coverlay flexible circuit was designed to make connections with the direct-write (DW) traces. In a processes developed by the investigators during the course of separate research, the flex circuit was bonded to the specimens first, then the DW traces were applied onto the specimens, including overwriting the flex-circuits (which included alignment marks). The flex circuit was designed in the shape of a rectangular frame, with flaps on all 4 inside edges with exposed pads for the DW process. The specimens fit inside the frame window with the top and bottom flap overlapping onto the front of the FFRP, and the left and right flap overlapping on the back of the FFRP. Traces are then routed along the edges of the frame to an 80 pin connector located on a bottom tab for hardware connection. This “flex-frame”, as seen in Figure 4, provides reliable, durable and consistent electrical continuity from traces to hardware, specifically because it eliminates all contract resistance issues. Finally, a PCB was designed to mate with this flex-frame, containing switches to multiplex the channels and simple and reliable connections for a multimeter probe and PC readout. After being instrumented, each FFRP specimen was progressively impacted at 15, 30 and 45 ft-lbs, using the same guided dropped weight setup, with in-and-out-of-plane resistance measured after each subsequent impact.

Figure 4: Photograph of flex-frame with FFRP sample

## 4 EXPERIMENTAL RESULTS

Following the impact to the all specimen, no damage was visible to the unaided eye. Two sets of data were collected before and after each impact: 1) in-plane between each parallel pair of adjacent traces, and 2) through-thickness at each grid point created by the virtual intersection of the perpendicular top and bottom surface traces. From these measurements, percent-resistivity change could be calculated for each path.

### 4.1 Proof-of-Concept Results

For the initial proof-of-concept specimen, microscopy revealed cracking in the laminate. For the in-plane resistance, the short trace average resistance was 9 Ω pre-impact. Following impact, while the outermost trace pairs on either side of the damage site along the x-axis showed < 10% change, the middle was consistently > 100%, as seen in Figure 5 (top). Minor changes < 1% were detected between long trace pairs. For the 56 through-thickness grid points, pre-impact resistance values averaged 20 Ω. As seen in Figure 5 (bottom), a clear change of > 100% was detected in the impacted region. Along the x-axis, between the measurement points for the long traces (left edge in Figure 5 (bottom)) and the damage site, < 10% change was observed. However on the opposite side of the damage site (right side of Figure 5 (bottom)), a constant resistance offset was introduced due to the presence of cracks across the electrodes.

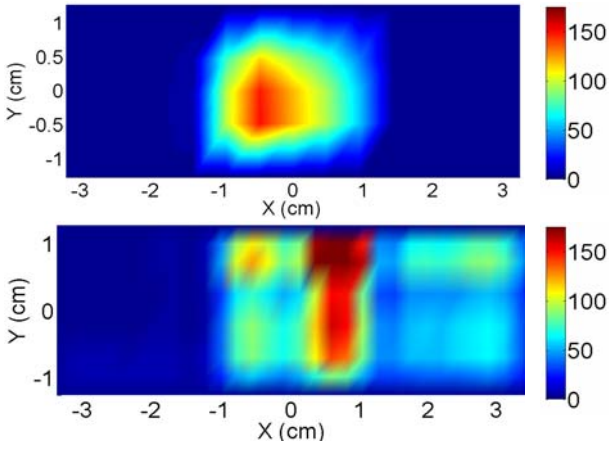


Figure 5: (Top) Visualization of in-plane resistance % change generated by multiplying & interpolating top/bottom adjacent parallel trace measurements. (Bottom) Visualization of through-thickness resistance % change generated by interpolating grid point measurements. Matlab was used to generate both images.

### 4.2 Validation Results

Subsequent to the completion of the initial test, 3 further validation tests, were performed to confirm the initial outcome with progressive impact energies. Following the procedure previously described, each of the 3 specimens were impacted at 15, 30 and 45 ft-lbs, with resistance data collected between each trial. Overall, the results from the refined setup served the intended purpose of validating the initial test results, demonstrating that the CNT's provide an excellent indication of barely visible impact damage (BVID). Furthermore, as seen in Figure 6, the overwhelming outcome was that with each progressive impact level additional breakage of CNT links caused a nearly linear increase in peak % change of resistance value.

For in-plane resistance, the first impact caused barely perceivable, but repeatable changes of ~10-20% in the impact region. The second impact caused ~20-30% resistance change, and the final impact ~40-60% change. In-plane results also appeared to be more localized to the actual impacted region, with clearly distinguishable damage patterns radiating from the impact center. Once locked into place, the impact location for progressive impacts on the same specimen was always in the same location, however due to some play in the guiding system for the dropped weight the impact location specimen-to-specimen was not always in the same location. This effect can be seen most dramatically by comparing specimen 2, which had the best central alignment, with specimen 3, which was impacted towards the bottom edge. The specimen-to-specimen variability in measured damage was also likely influenced by the actual impact point, as a central impact would be more uniformly distributed in the specimen and cause less edge crushing.

For through-thickness results, the initial impact again caused small changes of ~2-4%, with the second impact causing ~4-8% changes and the final impact registering ~8-10% changes. In this case, the pattern of the results appeared to be much less sensitive to impact location, likely because these were narrow specimens, however the damage severity measured did seem dependant on the impact point. It was also observed that the improved setup appeared to resolve the issue seen in the initial test results for the through-thickness measurements, where no DC off-set was calculated to the "right" of the damage region due to electrode cracking. No visible damage was present in any of these cases, however testing on witness specimens indicated that the specimens would completely fracture between 50-60 ft-lbs. The main difference in damage mode as compared to the initial specimen was the reduction from 2% to ~0.5% void fraction for these new specimens, likely concealing visible precursors to failure.

## 5 ALTERNATIVE METHODS

Beyond resistivity, other "alternative" CNT-based SHM and NDE methods were investigated. First, an AE approach was considered, exploiting the piezoresistive property of the CNTs to create an embedded network of acoustic sensors. Furthermore, it was demonstrated that nano-engineered laminates also have the potential to greatly enhance traditional non-destructive evaluation (NDE) methods such as thermography by virtue of their excellent electrical and thermal conductivity.

### 5.1 Acoustic Emission

Acoustic emission is a common SHM method used to passively detect impact events in a structure. Traditionally microphones, accelerometers or dedicated AE sensors are used to "listen" for high frequency stress waves (30-300 kHz) reverberating in the structure, radiating from the impact point. Triangulation can then be used to locate the impact point by using the time synchronized results from multiple sensors. The issue with this traditional method is that it requires many synchronous sensors distributed over a large area to cover an entire structure, and these types of sensors also typically have reliability concerns.

During the present research, CNT were used as embedded AE sensors. Essentially, as the CNT fibers are strained by the stress wave, their resistance value dynamically changes proportionately (as opposed to piezoelectric material where strain causes a voltage to be produced). Therefore, the response of the laminate to an impact event could be captured through the local CNT piezoresistive response captured over an electrode grid using a similar resistance measurement setup with higher frequency acquisition system. This approach will enable full-field visualization of the waves as they propagate from the point source. This may allow easy detection and location of damage. In addition, since this method would use high frequency data (>30 kHz), it would be much less susceptible to static, structural dynamic operating or acoustic loads, the effects of which can be filtered out in the frequency domain.

A proof of concept experiment was successfully conducted to demonstrate the feasibility of this approach. Using an undamaged FFRP specimen, a constant current source and an oscilloscope were connected to pairs of electrodes on either extreme of the specimen, in order to monitor the dynamic voltage response on the same time scale. Subsequently a pencil tip was broken in several places along the length of the specimen which would trigger the oscilloscope to capture data by the slight jump in voltage. By comparing the relative arrival times of the voltage peaks measured from either end of the specimen, the location of the pencil break could be easily determined.

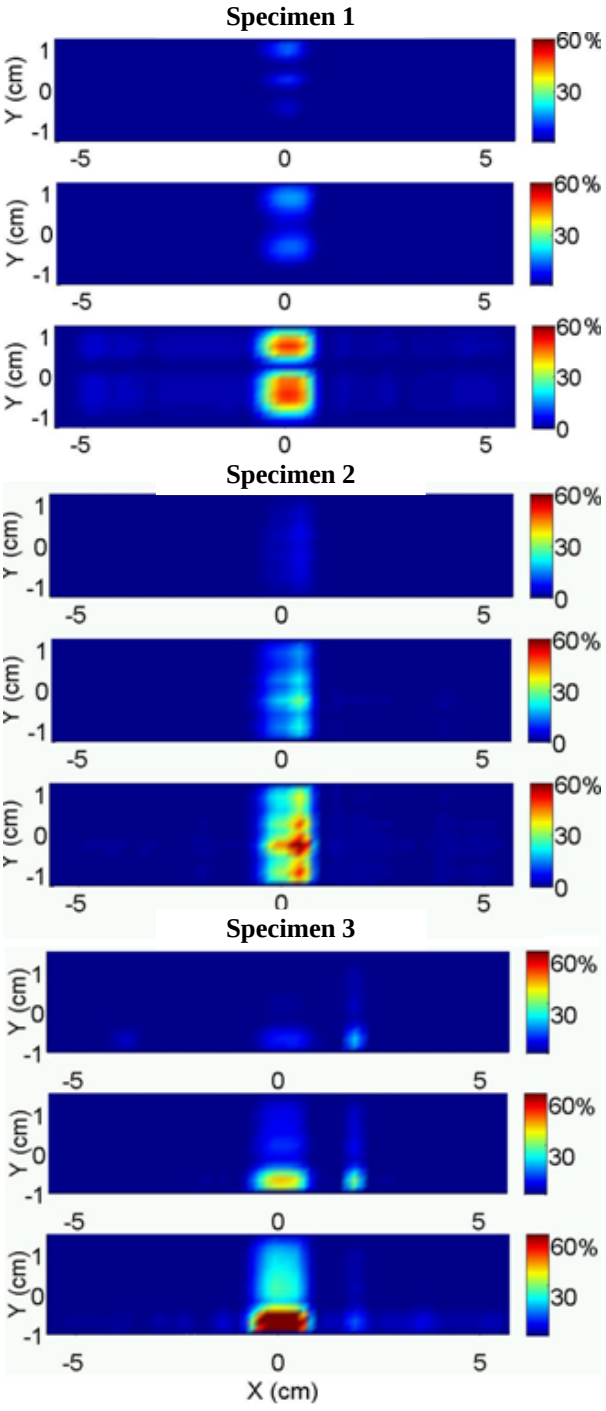


Figure 6 (a): Visualization of impact-induced % change for in-plane resistance values. First plot in each set presents changes following 15 ft-lbs impact, second follows 30 ft-lbs and third presents results following 45 ft-lbs impact. Matlab was used to generate all images.

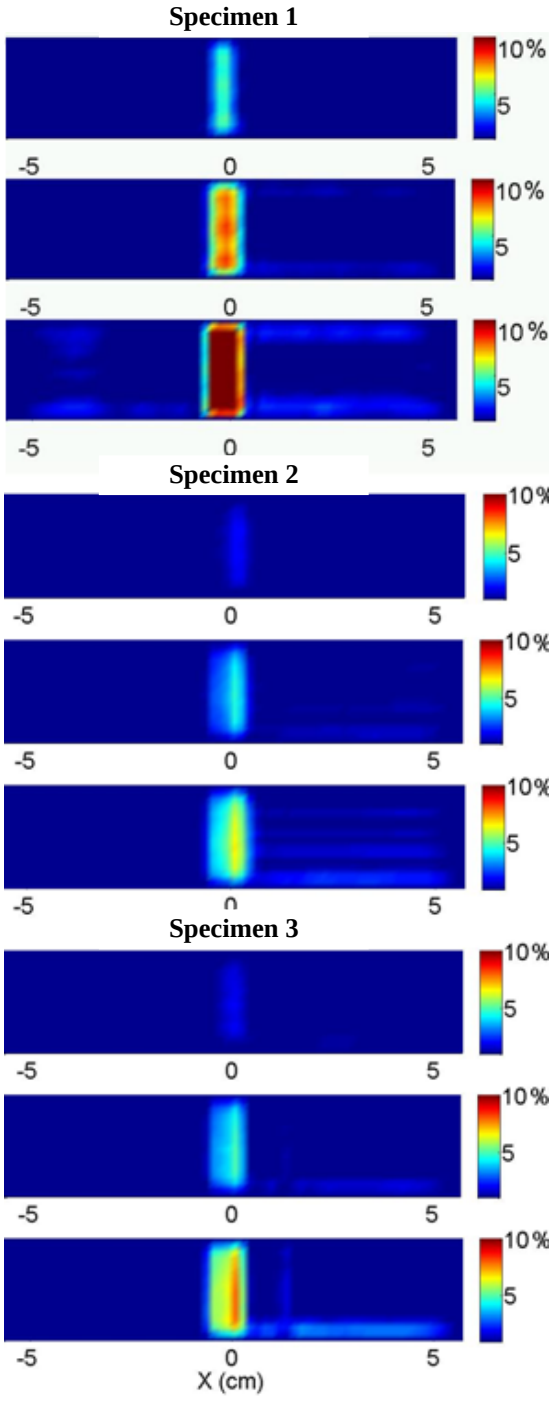


Figure 6 (b): Visualization of impact-induced % change for through-thickness resistance values. First plot in each set presents changes following 15 ft-lbs impact, second follows 30 ft-lbs and third presents results following 45 ft-lbs impact. Matlab was used to generate all images.

### 5.2 Thermography

Recently it was discovered that due to the nature of the CNTs having a reasonably low electrical resistance and high thermal conductivity, if a small voltage (volts) is placed across any electrode pair the FFRP would isothermally raise its temperature relevantly quickly (seconds). Furthermore, it was discovered that any Structural non-uniformities disrupt both the electrical and thermal flow in material, which could be recorded using convention thermographic imaging. Therefore these embedded CNT fibers could be used to greatly enhance thermography by providing a fast internal heating source, resolving a common issues thermography has in for detecting damage particularly in thick composite materials.

To explore thermographic damage detection, a simple proof-of-concept experiment was conducted using this method. As seen in Figure 7, a 2 V supply was placed across various electrode pairs on a previously impacted FFRP specimen while a simple thermal camera was used to capture the response. When the electrode pair away from the damage was utilized, no non-uniformities were observed beyond local heating near the electrodes. Subsequently, when the probes were placed at the extremes of the specimen, the impact damaged region became readily visible.

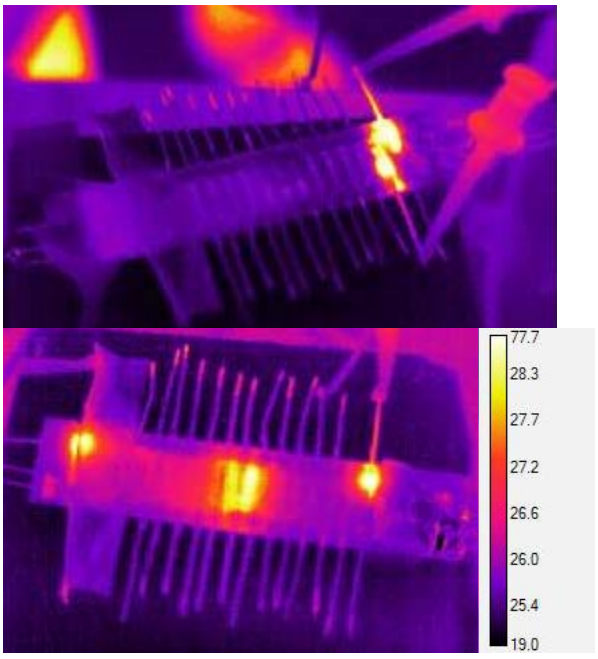


Figure 7: Thermographic images of impacted FFRP specimen. (Top) shows electrodes away from damage without any anomalies. (Bottom) Large anomaly is visible when electrode pair spans impact-damaged region. (Scale in degrees Celsius)

## 6 CONCLUSION

CNT-enhanced composites were fabricated, patterned with a silver ink electrode grid, and subsequently subjected to impact damage. Both in-plane and through-thickness electrical resistance measurements were collected. Clear changes were observed in both sets of data for grid lines close to the impacted zone of the specimen, demonstrating that these parameters were sensitive to damage in the structure. The peak changes were close to the center of the specimen near the impact site, and there was little to no change in values at points away from the damage zone. Overall, the sub-surface impact damage caused significant changes, allowing for a full-field representation of the damage locations by interpolating the collected data.

It is interesting to note that the results indicate that the parameters are sensitive to different damage modes, both from physical patterns and magnitude of resistance change. For instance, in-plane resistivity may be more sensitive to surface cracks, which tend to form at the edge of the impact zone. Conversely, through-thickness resistivity may be more sensitive to delamination, which would affect the CNT links across the specimen plies. This demonstrates the potential of using this approach as an SHM solution, with the added benefit of CNTs reinforcing the structure. In addition, proof-of-concept demonstrations for alternative SHM/NDE methods were also successfully achieved.

These results provide an excellent foundation for future research to further scale and mature this damage detection technology. Specific goals for continuing CNT-based SHM research includes optimization of electrode spacing with respect to damage sensitivity & resolution, investigating effects of load superposition such as temperature or mechanical on the resistance results, development of formal diagnostic algorithms and validation through probability of detection (POD) formulation. Expansion to other fiber system (such as carbon based laminates) and testing on larger scale built-up specimens is also of great interest

## ACKNOWLEDGMENT

This research regarding CNT-enhanced composite laminates for SHM was sponsored by Air Force Office of Scientific Research, under the Phase I SBIR contract FA9550-09-C-0165. Work was performed at Metis Design Corporation in Cambridge, MA in collaboration with the Massachusetts Institute of Technology in Cambridge, MA.

The FFRP composites used here were developed by MIT's Nano-Engineered Composite aerospace STructures (NECST) Consortium with support from Airbus S.A.S., Boeing, Embraer, Lockheed Martin, Saab AB, Spirit AeroSystems, Textron Inc., Composite Systems Technology, and TohoTenax.

**REFERENCES**


B. L. Ferrell (1999). JSF Prognostics and Health Management, *in Proceedings of IEEE Aerospace Conference*, Big Sky, MO.

Treacy M.M.J., Ebbesen T.W. and Gibson T.M. (1996) "Exceptionally high Young's modulus observed for individual carbon nanotubes," *Nature*, v. 381, pp. 680-687.

Salvetat J.P., Briggs G.A.D., Bonard J.M., Bacsa R.R., Kulik A.J. and Stockli T. (1999) "Elastic and shear moduli of single-walled carbon nanotube ropes," *Physical Review Letters*, v. 82(5), 944-947.

Yu M.F., Lourie O., Dyer M., Moloni K. and Kelly T. (2000). "Strength and breaking mechanism of multi-walled carbon nanotubes under tensile load," *Science*, v. 287, pp. 637-640.

Thostenson E.T., Ren Z. and Chou T.-W. (2001). "Advances in the science and technology of carbon nanotubes and their composites: a review," *Composite Science and Technology*, v. 61, pp. 1899-1912.

Wei B.Q., Vajtai R. and Ajayan P.M (2001). "Reliability and current carrying capacity of carbon nanotubes," *Applied Physics Letters*, v. 79, pp. 1172-4.

Zhang W., Suhr J. and Koratkar N. (2006) "Carbon nanotube/polycarbonate composites as multifunctional strain sensors," *Journal of Nanoscience and Nanotechnology*, v. 6, pp. 960-4.

Dharap P., Li Z.L., Nagarajaiah S. and Barrera E.V. (2004) "Nanotube film based on single-walled carbon nanotube for strain sensing," *Nanotechnology*, v. 15, pp. 379-82.

Ajayan P.M. and Tour J.M.(2007) "Nanotube composites," *Nature*, v. 447, pp. 1066-8.

Schulte K. and Windle A.H. (2007) Editorial, *Composite Science and Technology*, v. 67, pp. 777.

Gojny F.H., Wichmann M.H.G., et al. (2004) "Carbon nanotube-reinforced epoxy composites: enhanced stiffness and fracture toughness at low nanotube content," *Composite Science and Technology*, v. 64, pp. 2363-71.

Qiu, J., et al., (2007) *Carbon nanotube integrated multifunctional multiscale composites.* Nanotechnology, **18**(27), p. 275708.

Veedu V.P., Cao A., Li X., Ma K, Solano C., Kar S. et al. (2006) "Multifunctional composites using reinforced laminae with carbon-nanotube forests," *Nature Materials*, v. 5, pp. 457-62.

Beyakrova E., Thostenson E.T., Yu A., Kim H., Gao J., Tang J. et al. (2007) "Multiscale carbon nanotube-carbon fiber reinforcement for advanced epoxy composites," Langmuir, v. 23, pp. 3970-4.

Zhu J., Imam A., et al, (2007). "Processing a glass fiber reinforced vinyl ester composite with nanotube enhancement of interlaminar shear strength," *Composite Science and Technology*, v. 67, pp. 1509-17.

Yi Y.B., Berhan L., Sastry A.M. (2004). "Statistical geometry of random fibrous networks, revisited: waviness, dimensionality, and percolation," *Journal of Applied Physics*, v. 96(3), pp. 1318-27.

Du F.M., Fischer J.E., Winey K.I. (2004). "Effect of nanotube alignment on percolation conductivity in carbon nanotube/polymer composites," *Physical Review B*, v. 72(12), pp. 121404

Thostenson E.T. and Chou T.-W, (2006). "Carbon nanotube networks: sensing of distributed strain and damage for life prediction and self healing," *Advanced Materials*, v. 18, pp. 2837-41.

Garcia E.J., Wardle B.L., Hart J.A. and Yamamoto N. (2008). "Fabrication and multifunctional properties of a hybrid laminate with aligned carbon nanotubes grown *in situ*," *Composite Science and Technology*, v. 68, pp. 2034-41.

Fiedler B., Gojny F. H. and M. H. G. Wichmann, W. Bauhofer, K. Schulte, (2004).*Annales de Chimie Science des Matériaux*, *22*, 81.

Thostenson E. T. andT.-W. Chou, (2006).*Adv. Mater. 18*, 2837.

Ahmed T. J., Nino G. F., Bersee H. E. N. and A. Beukers, (2008).*Composites Part A 39*, 1025.

Hung Y. Y., Chen Y. S., Ng S. P., Liu L., Huang Y. H., Luk B. L., Ip R. W. L., Wu C. M. L., and P. S. Chung, (2009).*Materials Science and Engineering: R: Reports*, *64*, 73.

Kumar J., Baby S. and V. Kumar, (2008).*Materials Science and Engineering: A*, *496*, 303.

Hellier C. (2001). (Ed: M.-H. Professional), 603.

Roach D., (2008).*High-Performance Composites 16*, 72.

Guzman de Villoria R., Wardle, B.L. and A. Miravete, (2009). "Systems and Methods for Structural Sensing", MIT TLO Case 13988, U.S. Provisional Patent Application 61/262,864.

Kessler S.S., Raghavan A. and B.L. Wardle "Multifunctional CNT-Engineered Structures," MIT TLO Case 14127, U.S. Provisional Patent Application 61/298,385.

Guzman de Villoria, R., Yamamoto, N., Miravete, A., and B.L. Wardle, (2010). "Preventing Catastrophic Failures: Multi-Physics Materials for Damage Detection," submitted May 2010.